LETTER

doi:10.1038/nature12363

Seasonal sea surface cooling in the equatorial Pacific cold tongue controlled by ocean mixing

James N. Moum[1], Alexander Perlin[1]‡, Jonathan D. Nash[1] & Michael J. McPhaden[2]

Sea surface temperature (SST) is a critical control on the atmosphere[1], and numerical models of atmosphere–ocean circulation emphasize its accurate prediction. Yet many models demonstrate large, systematic biases in simulated SST in the equatorial 'cold tongues' (expansive regions of net heat uptake from the atmosphere) of the Atlantic[2] and Pacific[3] oceans, particularly with regard to a central but little-understood feature of tropical oceans: a strong seasonal cycle. The biases may be related to the inability of models to constrain turbulent mixing realistically[4], given that turbulent mixing, combined with seasonal variations in atmospheric heating, determines SST. In temperate oceans, the seasonal SST cycle is clearly related to varying solar heating[5]; in the tropics, however, SSTs vary seasonally in the absence of similar variations in solar inputs[6]. Turbulent mixing has long been a likely explanation, but firm, long-term observational evidence has been absent. Here we show the existence of a distinctive seasonal cycle of subsurface cooling via mixing in the equatorial Pacific cold tongue, using multi-year measurements of turbulence in the ocean. In boreal spring, SST rises by 2 kelvin when heating of the upper ocean by the atmosphere exceeds cooling by mixing from below. In boreal summer, SST decreases because cooling from below exceeds heating from above. When the effects of lateral advection are considered, the magnitude of summer cooling via mixing (4 kelvin per month) is equivalent to that required to counter the heating terms. These results provide quantitative assessment of how mixing varies on timescales longer than a few weeks, clearly showing its controlling influence on seasonal cooling of SST in a critical oceanic regime.

Equatorial cold tongues in the Atlantic and Pacific are formed in part through diverging horizontal transport near the sea surface associated with large-scale wind patterns, which bring cool waters towards the ocean surface[7,8]. Maintaining cool SSTs in the presence of intense solar heating requires a combination of subsurface mixing and vertical advection to transport surface heat downward[4,9–11]. Limited measurements during the passage of a tropical instability wave (TIW) at 0, 140° W revealed a tenfold increase in subsurface turbulent heat flux[12]. This was sufficient to cool surface waters by 2 K per month, indicating that mixing alone has the potential to maintain the equatorial cold tongue, a conjecture supported by climatological evidence that sea surface cooling is enhanced by TIWs[12].

Establishing general relationships that show how irreversible turbulent mixing influences patterns in large-scale (10,000 km) ocean phenomena has been notoriously difficult for two reasons. First, the delicate measurements required to quantify mixing have been limited to short shipboard campaigns (30 days) that target specific processes[13–17]. Although these have led to fundamental advances in our knowledge of ocean dynamics at a few locations and on timescales of a few weeks, such measurements are unable to determine whether changes in mixing on seasonal and interannual timescales might influence large-scale dynamics. Second, diagnostics of mixing in numerical model solutions of ocean circulation are ambiguous, because models grossly oversimplify their representation of mixing, which occurs on scales that are orders of magnitude smaller than the smallest spatial and shortest timescales resolved.

Here we directly quantify variations in mixing on long timescales using specialized instrumentation that we developed for use on oceanographic moorings[18,19]. Since late 2005, these sensors have provided near-continuous measurements of mixing below the Tropical Atmosphere–Ocean (TAO) buoy maintained by the National Ocean and Atmospheric Administration (NOAA) at 0, 140° W[20].

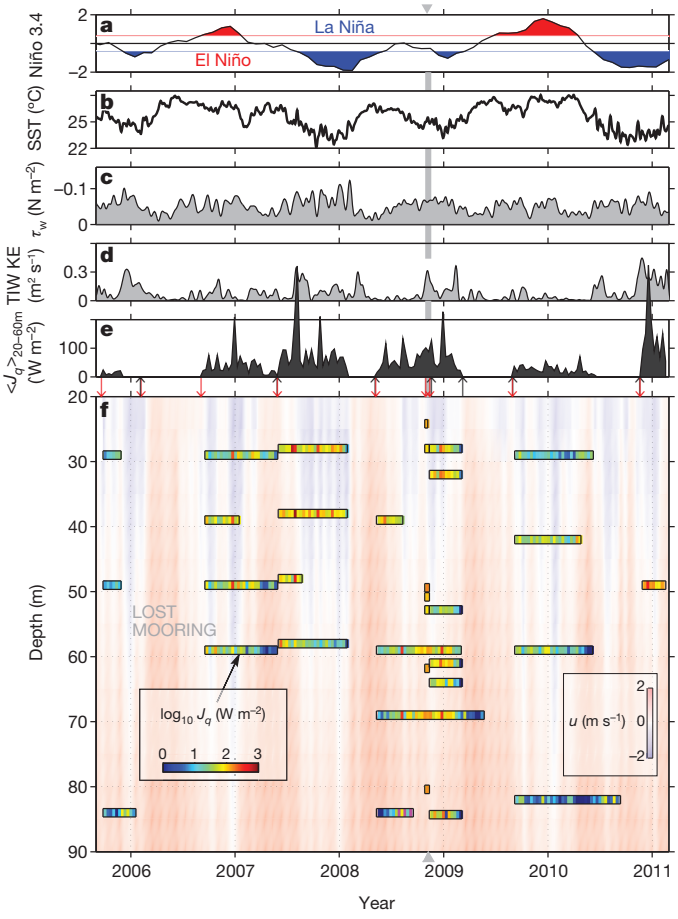

Figure 1 | Six-year record of mixing at the TAO mooring at 0, 140° W. **a**, Niño3.4 SST index, a measure of the relative strengths of El Niño and La Niña events[28]. **b**, SST. **c**, Wind stress, τ_w (7-day averages). **d**, Squared meridional velocity at 40 m filtered at 12–33 days, taken as a proxy for kinetic energy in the tropical instability wave frequency band (TIW KE). **e**, Turbulent heat flux averaged over depths 20–60 m, $<J_q>_{20\text{-}60m}$. **f**, Image plot of zonal currents (zonal velocity denoted u, eastward currents red, westward blue; see right inset colour scale). Coloured bars show depths and durations of χ-pod deployments; $\log_{10} J_q$ is indicated by the colour (10-day average, see left inset colour scale). Arrows at top of **f** show deployments (red) and recoveries (black) of moorings. Grey bars show period of comparison experiment with shipboard turbulence profiling instrumentation[12,19].

[1]College of Earth, Ocean and Atmospheric Sciences, Oregon State University, Corvallis, Oregon 97331, USA. [2]NOAA/Pacific Marine Environmental Laboratory, Seattle, Washington 98115, USA. ‡Deceased.

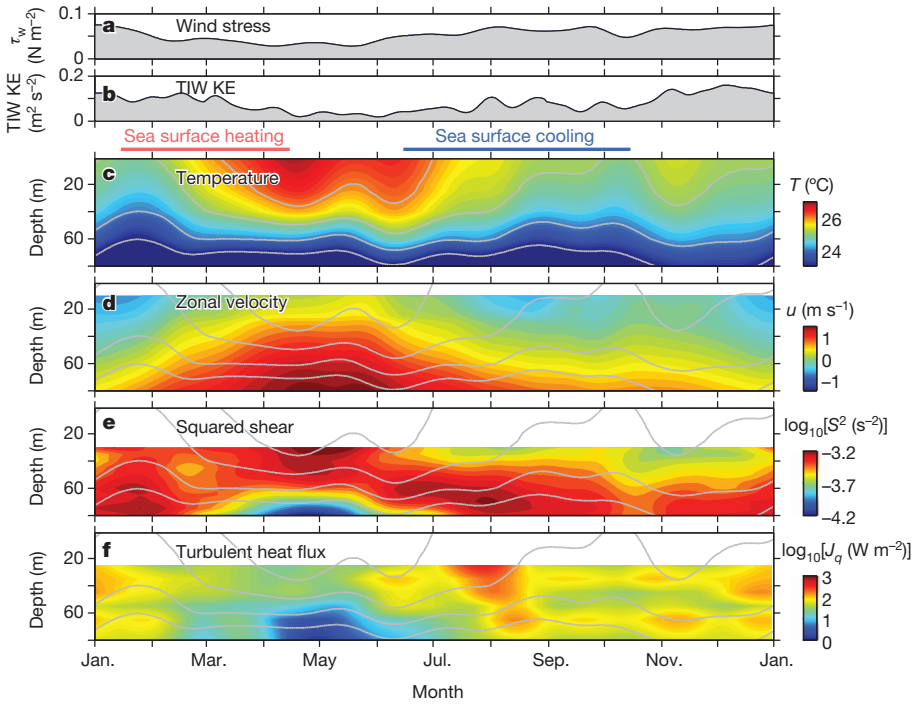

Figure 2 | Annual cycles of upper-ocean vertical structure at 0, 140° W over the period 2005–11. **a**, τ_w; **b**, TIW KE; **c**, T; **d**, zonal velocity, u; **e**, $\log_{10}S^2$, where $S^2 = u_z^2 + v_z^2$; **f**, $\log_{10}J_q$. Velocities from upward-looking subsurface acoustic Doppler current profiler measurements at 270 m nominal depth go up to 30 m depth at 5 m vertical bin spacing. Point velocity measurements at 10 m depth extend velocities closer to the surface but are not used in estimation of S^2. Grey contours in **c** are isotherms, which are transferred onto **d**–**f** for reference.

This first multi-year time series of mixing is summarized in Fig. 1f together with other measures of larger-scale background influences (Fig. 1a–d). Considered together, these suggest patterns in mixing that span multiple depth ranges on timescales of weeks to months, contributing to a cyclic pattern of mixing on the seasonal timescale (Fig. 1f), and hint at longer-timescale patterns (for example, mixing is weaker during El Niño events than during La Niña events or neutral periods; Fig. 1a, e). Short-timescale variations associated with shear instabilities[21,22], daily cooling[13,14] and weekly variations in surface winds[13] are hidden by our 10-day averaging. Our intent here is to establish the role of mixing on the seasonal cycle.

As a metric to quantify long-term patterns, we compute the turbulent heat flux (J_q, coloured bars in Fig. 1f and defined in Methods) averaged over 20–60 m depth ($<J_q>_{20\text{-}60\text{m}}$; Fig. 1e). Over this depth range, turbulence fluctuations are closely related to coupled air–sea interactions, and to strong velocity gradients formed between the westward flowing near-surface South Equatorial Current (SEC) and the core of the Equatorial Undercurrent (maximum eastward flow near 100 m; 95% confidence interval CI = 70–145 m) are marginally stable, offering an additional energy source for mixing.

From monthly-averaged data, $<J_q>_{20\text{-}60\text{m}}$ is positively correlated with wind stress ($r = 0.43$, 95% CI = 0.15–0.64, P-value $P = 0.004$) and TIW kinetic energy (KE; $r = 0.59$, 95% CI = 0.35–0.75, $P = 0.00002$). However, it is not significantly correlated, on a monthly average, with any available measure of vertical stratification, shear, or their ratio, Ri (the gradient Richardson number, which defines the instability condition for stratified shear flows). Such correlations do exist in high-resolution measurements from targeted process experiments[21,23], suggesting that the averaging over long periods hides the mechanistic relationships that drive the turbulence. Regardless, strong seasonal cycles exist in all flow properties of the equatorial cold tongue (Fig. 2), including clear correspondences between J_q, shear and stratification. Warming of the upper 50 m in boreal spring coincides with reduced winds, weakening or disappearance of the westward flowing SEC, and reduced TIW KE; J_q is diminished throughout the water column. Increasing winds and TIW KE occur in late summer, following which the SEC reappears, the layer of high shear deepens, J_q increases and surface waters cool. Despite continued high wind stress (τ_w) in September, J_q weakens throughout the upper water column, as does velocity shear in the upper 60 m. High τ_w and high TIW KE accompany a secondary maximum in J_q late in the year.

The quantity $<J_q>_{20\text{-}60\text{m}}$ (Fig. 3a) exhibits an annual cycle that is significant at the 95% confidence level. Minima in April–May are a factor of 6 smaller than the maximum in August. The smallest values of $<J_q>_{20\text{-}60\text{m}}$ coincide with rising or maximum SST and the largest values with cooling SST.

We examine the heat budget of the surface mixed layer (with depth h) to illustrate the importance of J_q to changes in SST. The net surface flux acting to heat or cool the mixed layer is $J_q^0 - I^h$ (Fig. 3a), where J_q^0 is the total surface flux from atmosphere to ocean and I^h is the intensity of short wave radiation penetrating below h. J_q^0 is determined from the TropFlux analysis[6], I^h is derived from an empirical formulation[24], and h is determined from hourly temperature profile measurements on the TAO mooring (Supplementary Information). In the annual cycle, $J_q^0 - I^h$ peaks in late boreal winter with a minimum in late boreal summer[9]. The critical seasonal modulation of $J_q^0 - I^h$ is due in equal parts to modulations of solar radiation and latent cooling (a seasonal cycle of atmospheric flux components is included in Supplementary Information) but is partially offset by I^h, which is diminished in boreal summer when winds and mixing tend to increase h.

The heating and cooling rate of a fluid parcel due solely to vertical mixing is $\rho C_p \mathrm{d}T/\mathrm{d}t = -\mathrm{d}J_q/\mathrm{d}z$, where ρ, C_p and T are respectively the density, heat capacity and temperature of the fluid parcel, t is time and $\mathrm{d}J_q/\mathrm{d}z$ the vertical heat flux divergence across the fluid parcel. Across the surface mixed layer $\mathrm{d}J_q/\mathrm{d}z = (J_q^0 - I^h - J_q^h)/h$, where J_q^h is the turbulent heat flux acting across the mixed layer base. If we assume that $<J_q>_{20\text{-}60\text{m}}$ is a reasonable estimator of J_q^h, then the sign of $<J_q>_{20\text{-}60\text{m}} - (J_q^0 - I^h)$ in Fig. 3a ought to reflect the sign of the observed cooling rate, $\mathrm{dSST}/\mathrm{d}t$. During February to May, $J_q^0 - I^h > J_q^h$, coincident with maximum sea surface heating. Conversely, from June to September, $J_q^0 - I^h < J_q^h$, coinciding with maximum sea surface cooling. The maximum observed cooling rate is <1 K month^{-1} while the heat flux divergence based on mixing alone contributes a maximum cooling of 4 K month^{-1} (Fig. 3b).

The surface mixed layer heat budget discussed above considered a one-dimensional vertical balance. However, at the fixed point of observation, SST is also changed by horizontal advection[25]: gradients in temperature transported by surface currents cause a local change in temperature (see Supplementary Information). The sign of the zonal

advection (uT_x) varies with that of the zonal surface currents (u) because the negative sign of the zonal SST gradient (T_x) is relatively constant. Meridional advection (vT_y), largely due to TIWs, is a net heat source (Fig. 3b). Vertical advection (upwelling) brings cool fluid nearer the surface but mixing is required to modify SST. The sum of heat flux divergence and advection balances the observed heating rate (within 95% confidence limits) during strong sea surface cooling (July–September), but indicates greater heating than observed at other times.

Vertical profiles of $J_q^h(z)$, averaged on seasonal timescales (Fig. 4), show that the heat flux during June–August has significant vertical structure coincident with minimal $J_q^0 - I^h$, suggesting that the flux divergence acting across the sea surface may actually be larger than shown in Fig. 3b. It also emphasizes the distinctively weak turbulence throughout the upper 70 m in March–May, the period coinciding with maximal $J_q^0 - I^h$.

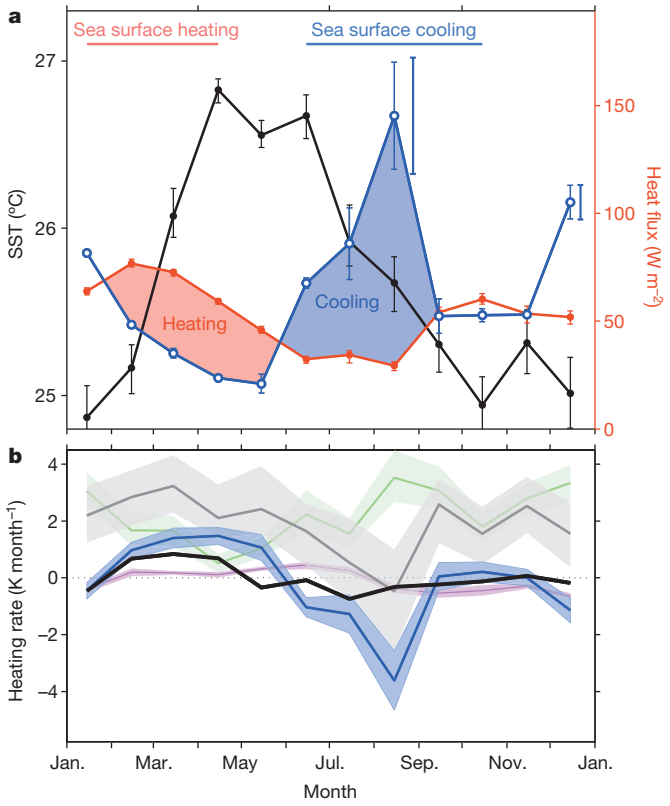

Figure 3 | Annual cycles of SST and turbulence at 0, 140° W. a, SST (black), $<J_q>_{20\text{-}60m}$ (blue) and that part of the surface heat flux that contributes to mixed layer heating ($J_q^0 - I^h$) from TropFlux (red; http://www.locean-ipsl.upmc.fr/tropflux/). Averages are derived from the observations in Fig. 1. Error bars on SST and $J_q^0 - I^h$ are 95% confidence limits on bootstrap estimates of means from daily values. Error bars on individual values of $<J_q>_{20\text{-}60m}$ represent the range based on two independent estimates of T_z. One estimate is computed from the temperature profile the sensor measures as it profiles the water column by surface-wave-induced motion coupled through the surface float. The second estimate uses temperature profiles from auxiliary temperature sensors distributed about that χ-pod on the mooring, averaged hourly in time and differenced vertically over 10–20 m. The value of J_q plotted is the average of these two estimates. Natural variability is represented by 95% bootstrap confidence intervals on 15-min averages of J_q for the largest (August) value by the adjacent blue bar, and for all of the data by the blue bar adjacent to the December value. Details are included in Supplementary Information. **b**, Terms contributing to SST evolution. Black line, dSST/dt; blue, $1/(\rho Cp)\mathrm{d}J_q/\mathrm{d}z$; red, uT_x; green, vT_y; grey, $1/(\rho C_p)\mathrm{d}J_q/\mathrm{d}z + uT_x + vT_y$. Advection terms uT_x, vT_y were computed from surface currents measured at the mooring and a revised SST product[29]. Uncertainties (shaded regions) are 95% bootstrap confidence limits on means computed from 30-day averages. Confidence limits on the turbulent heat flux divergence are based on reasonable ranges of h (Supplementary Information).

The finding that $J_q^0 - I^h$ and J_q^h are each in quadrature with SST but out-of-phase with each other is a critical factor in defining the seasonal cycle of SST. The strong correlation between mixing and wind stress on the annual cycle, together with correlations found over shorter periods[13], suggests the importance of the (predominantly easterly) wind in enhancing westward currents, thereby increasing velocity gradients and promoting shear instability, which is likely to be the root cause of turbulence in the upper equatorial ocean[21,22,26]. Higher winds also increase latent cooling, decreasing $J_q^0 - I^h$ at the same times that mixing peaks.

These are, to our knowledge, the first long-term mixing measurements in the ocean that resolve the temporal intermittency and multi-year variability at a point of observation. Figure 3a clearly shows that observed seasonal sea surface heating and cooling coincide with the correct sign of the air–sea heat flux divergence. Subsurface mixing is the dominant sea surface cooling term and controls the SST cooling phase, but provides too little cooling to counter surface heating from the atmosphere plus advection during some parts of the year. It is possible that, at these times, the governing heat flux divergence is shallower than 20 m, as suggested by Fig. 4. It is also possible that spatial intermittency is important because the measured temperature of a fluid parcel is controlled by the cumulative sum of the mixing processes along its trajectory. Spatial gradients in temperature and currents are large, especially across the Equator. Gradients in mixing are unknown, but if they are proportionately large, then fluid parcels at the point of observation may have experienced a different history of mixing than observed.

This finding—that equatorial mixing is organized in a meaningful seasonal cycle—shows that the ocean's microstructure (on scales of seconds to minutes and centimetres to metres) is clearly linked to, and at times dominates, particular aspects of the larger-scale dynamics. Extended measurements like these are intended to provide quantitative estimates of mixing on interannual timescales to improve our understanding of the El Niño/Southern Oscillation cycle and help to

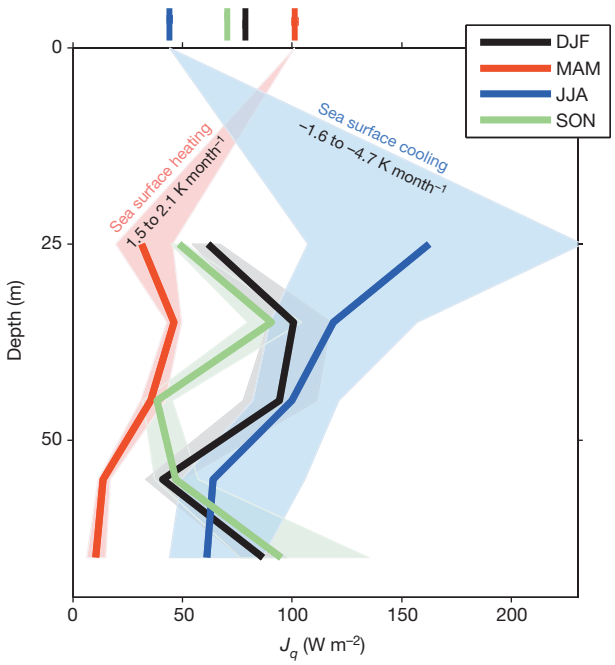

Figure 4 | Seasonally averaged vertical profiles of turbulence heat flux. Curves are shown for December–February (DJF); March–May (MAM); June–August (JJA) and September–November (SON). Positive heat flux indicates heating from above. Shading indicates 95% bootstrapped confidence limits on means based on 15-min averages. At top, values of $J_q^0 - I^h$ in W m^{-2} are shown as vertical bars.

reduce the equatorial Pacific cold tongue bias that affects the mean state of many coupled ocean–atmosphere climate models[3].

METHODS SUMMARY

The vertical (more strictly, diapycnal) flux of heat by turbulence is represented by Fickian diffusion, enhanced by a turbulence diffusion coefficient, $K_\rho = \chi_T/T_z^2$ (ref. 27). The temperature variance dissipation rate (χ_T) is computed by scaling the temperature gradient spectrum measured by fast thermistors on small autonomous instruments ('χ-pods')[18] attached to oceanographic moorings and packaged with inertial navigation units to quantify the component of flow speed past the sensor that is due to wave-induced motions of the surface float[19]. The other component of the flow speed is the ocean current speed, measured separately by velocity sensors on the mooring. The vertical temperature gradient, T_z, is defined locally by the vertical motion of the sensor through the water or, on a larger scale, by additional temperature sensors on the mooring. The depth-dependent vertical heat flux caused by turbulence is $J_q = -\rho C_p K_\rho T_z$.

Received 14 March; accepted 3 June 2013.
Published online 24 July 2013.

1. Xie, S.-P. Satellite observations of cool ocean-atmosphere interaction. *Bull. Am. Meteorol. Soc.* **85,** 195–208 (2004).
2. Richter, I. & Xie, S.-P. On the origin of equatorial Atlantic biases in coupled general circulation models. *Clim. Dyn.* **31,** 587–598 (2008).
3. Wittenberg, A. T., Rosati, A., Lau, N. C. & Ploshay, J. J. GFDL's CM2 global coupled climate models. Part III: Tropical Pacific climate and ENSO. *J. Clim.* **19,** 698–722 (2006).
4. Jouanno, J., Marin, F., Du Penhoat, Y., Sheinbaum, J. & Molines, J.-M. Seasonal heat balance in the upper 100 m of the equatorial Atlantic ocean. *J. Geophys. Res.* **116,** C09003 (2011).
5. Xie, S. On the genesis of the equatorial annual cycle. *J. Clim.* **7,** 2008–2013 (1994).
6. Praveen Kumar, B., Vialard, J., Lengaigne, M., Murty, V. S. N. & McPhaden, M. J. TropFlux: air-sea fluxes for the global tropical oceans—description and evaluation. *Clim. Dyn.* **38,** 1521–1543 (2012).
7. Mitchell, T. P. & Wallace, J. M. The annual cycle in equatorial convection and sea surface temperature. *J. Clim.* **5,** 1140–1156 (1992).
8. Trenberth, K. E., Caron, J. M. & Stepaniak, D. P. The atmospheric energy budget and implications for surface fluxes and ocean heat transports. *Clim. Dyn.* **17,** 259–276 (2001).
9. Wang, B. & Fu, X. Processes determining the rapid reestablishment of the equatorial Pacific cold tongue/ITCZ complex. *J. Clim.* **14,** 2250–2265 (2001).
10. Wang, W. & McPhaden, M. J. The surface-layer heat balance in the equatorial Pacific ocean. Part I: mean seasonal cycle. *J. Phys. Oceanogr.* **29,** 1812–1831 (1999).
11. McPhaden, M. J., Cronin, M. F. & McClurg, D. C. Meridional structure of the seasonally varying mixed layer temperature balance in the eastern tropical Pacific. *J. Clim.* **21,** 3240–3260 (2008).
12. Moum, J. N. *et al.* Sea surface cooling at the Equator by subsurface mixing in tropical instability waves. *Nature Geosci.* **2,** 761–765 (2009).
13. Moum, J. N. & Caldwell, D. R. Local influences on shear flow turbulence in the equatorial ocean. *Science* **230,** 315–316 (1985).
14. Gregg, M. C., Peters, H., Wesson, J. C., Oakey, N. S. & Shay, T. J. Intensive measurements of turbulence and shear in the equatorial undercurrent. *Nature* **318,** 140–144 (1985).
15. Lien, R.-C., Caldwell, D. R., Gregg, M. C. & Moum, J. N. Turbulence variability in the central Pacific at the beginning of the 1991–93 El Niño. *J. Geophys. Res.* **100,** 6881–6898 (1995).
16. Inoue, R., Lien, R.-C. & Moum, J. N. Modulation of equatorial turbulence by a tropical instability wave. *J. Geophys. Res.* **117,** C10009 (2012).
17. Hummels, R. & Dengler, M. B. B. Seasonal and regional variability of upper ocean diapycnal heat flux in the Atlantic cold tongue. *Prog. Oceanogr.* **111,** 52–74 (2013).
18. Moum, J. N. & Nash, J. D. Mixing measurements on an equatorial ocean mooring. *J. Atmos. Ocean. Technol.* **26,** 317–336 (2009).
19. Perlin, A. & Moum, J. N. Comparison of thermal variance dissipation rates from moored and profiling instruments at the equator. *J. Atmos. Ocean. Technol.* **29,** 1347–1362 (2012).
20. McPhaden, M. J. *et al.* The tropical ocean-global atmosphere observing system: a decade of progress. *J. Geophys. Res.* **103,** 14,169–14,240 (1998).
21. Moum, J. N., Nash, J. D. & Smyth, W. D. Narrowband high-frequency oscillations at the equator. Part I: interpretation as shear instabilities. *J. Phys. Oceanogr.* **41,** 397–411 (2011).
22. Smyth, W. D., Moum, J. N., Li, L. & Thorpe, S. A. Shear instability, the descent of the diurnal mixing layer and the deep cycle of equatorial turbulence. *J. Phys. Oceanogr.* (submitted).
23. Zaron, E. D. & Moum, J. N. A new look at Richardson number mixing schemes for equatorial ocean modeling. *J. Phys. Oceanogr.* **39,** 2652–2664 (2009).
24. Ohlmann, J. C., Siegel, D. A. & Gautier, C. Ocean mixed layer radiant heating and solar penetration: a global analysis. *J. Clim.* **9,** 2265–2280 (1996).
25. Swenson, M. S. & Hansen, D. V. Tropical Pacific ocean mixed layer heat budget: the Pacific cold tongue. *J. Phys. Oceanogr.* **29,** 69–81 (1999).
26. Sun, C., Smyth, W. D. & Moum, J. N. Dynamic instability of stratified shear flow in the upper equatorial ocean. *J. Geophys. Res.* **103,** 10323–10337 (1998).
27. Osborn, T. R. & Cox, C. S. Oceanic fine structure. *Geophys. Fluid Dyn.* **3,** 321–345 (1972).
28. NOAA Commerce Department. NOAA gets U.S. consensus for El Niño/La Niña index, definitions. *NOAA press release NOAA 03–119* (2003); available at http://www.noaanews.noaa.gov/stories/s2095.htm.
29. Reynolds, R. W. *et al.* Daily high-resolution-blended analyses for sea surface temperature. *J. Clim.* **20,** 5473–5496 (2007).

Supplementary Information is available in the online version of the paper.

Acknowledgements This work was funded by the National Science Foundation (grants 0424133, 0728375 and 1256620). We thank M. Neeley-Brown and R. Kreth, who were primarily responsible for construction, testing and maintenance of χ-pods, and P. Freitag and NOAA's PMEL mooring group, who helped us to get started with these measurements. We also thank NOAA's NDBC group, who have continued to deploy our χ-pods on TAO moorings. E. Shroyer, S. de Szoeke, K. Benoit-Bird and D. Chelton provided comments on the paper. This is PMEL contribution no. 3970. We dedicate this paper to the memory of our colleague and co-author A. Perlin, who passed away during final revisions, and to the memory of lab engineer R. Kreth.

Author Contributions J.N.M. wrote the paper. A.P. and J.N.M. did the analysis. J.D.N. has been part of this project since its inception and provided suggestions for analysis. M.J.M. provided advice on the large-scale context of these measurements. All authors contributed suggestions and text at the writing stage.

Author Information Reprints and permissions information is available at www.nature.com/reprints. The authors declare no competing financial interests. Readers are welcome to comment on the online version of the paper. Correspondence and requests for materials should be addressed to J.N.M. (moum@coas.oregonstate.edu).